STM JOURNALS

Journal of
Polymer & Composites

ISSN: 2321-2810 (Online)
ISSN: 2321-8525 (Print)
Volume 13, Issue 6, 2025
DOI (Journal): 10.37591/JoPC

https://journals.stmjournals.com/jopc/

Research JoPC

Optimization of Direct Ink Writing Process Parameters for Liquid Silicone Rubber/TiO_2 Composite Ink

Jhunjhun Kumar Mishra[1]*, Vishal Francis[2]

Abstract

The purpose of this research is to develop and optimize the Liquid Silicone Rubber (LSR)/Titanium Dioxide (TiO_2) composite inks in Direct Ink Writing (DIW)-based 3D printing systems. The primary research objective was to use enhancement of mechanical, rheological, and dielectric characteristics of LSR using TiO_2 reinforcement but still retain extrusion stability and dimensional consistency. TiO_2 content (0, 5, 10, and 15 wt%) and catalyst and glycerol ratios were regulated and were used to prepare four ink formulations. To determine the structure-property relationships, the materials have been and were characterized through rotational rheometry, FTIR spectroscopy, X-ray diffraction (XRD), and scanning electron microscopy (SEM). From the analysis, it was found out that the 5 wt% TiO_2 composition displayed the best rheological characteristics with shear-thinning viscosity, which allowed DIW extrusion, good dispersion of the nanoparticle, and good adhesion of the particles to the silicone matrix. SEM analysis proved to be homogenous and possessing low agglomeration at this concentration, and XRD and FTIR confirmed stability of the phases and chemical compatibility of TiO_2 and LSR. Part fabrication experiments further confirmed rapid extrusion, smooth deposition, and high dimensional fidelity at 390 mm/min print speed and 60° substrate temperature. The overall results of the research identify the LSR/TiO_2 (5 wt%) as the best formulation in the functional elastomeric 3D printing with better print quality, mechanical strength, and printability reliability in flexible electronics and biomedical applications.

Keywords: Direct Ink Writing, Liquid Silicone Rubber, Titanium Dioxide, Dielectric Properties, SEM

INTRODUCTION

Direct Ink Writing (DIW) is an extrusion-based additive manufacturing technology that allows creation of complex three-dimensional geometries by means of layer-based deposition of paste like ink under determined shear and extrusion conditions [1]. DIW is being used to fabricate functional soft devices due to the ability to deposit multimaterial, localized property modifications and fillers integration to control electrical, mechanical and thermal properties [2]. Liquid silicone rubber (LSR) is a preferable DIW feedstock in soft robotics, wearable sensors and biomedical sensors because of its flexibility, biocompatibility, chemical stability, and thermal stability [3], [4]. Nonetheless, native LSR is lacks dielectric functionality as well as reinforcing prowess; thus, addition of high-permittivity inorganic fillers like titanium dioxide (TiO_2) is being explored to confer dielectric, thermal and mechanical functionality and remain DIW printable [5]-[7]. To produce such LSR/TiO_2 inks, particle and matrix interaction, dispersion stability, viscosity, shear-thinning properties have to be controlled to maintain extrusion fidelity and interlayer adhesion [8], [9]. According to recent research, moderate

***Author for Correspondence**
Jhunjhun Kumar Mishra
E-mail: jkumarmishra8@yahoo.com

[1]PhD Research Scholar, School of Mechanical Engineering, Lovely Professional University, Punjab, Phagwara, 144411, India
[2]Associate Professor, School of Mechanical Engineering, Lovely Professional University, Punjab, Phagwara, 144411, India

Received Date: November 04, 2025
Accepted Date: November 12, 2025
Published Date: November 22, 2025

Citation: Author. Optimization of Direct Ink Writing Process Parameters for Liquid Silicone Rubber/TiO_2 Composite Ink. Journal of Polymer & Composites. 2025; 13(6): 240–259p.

nanoparticle loading enhances mechanical reinforcement and dielectric response and excessive loading causes agglomerated properties, irregular rheology and low print fidelity [10]. Having proceeded with the research work, a number of prevailing research were critically examined and is below in sequencing:

Foerster et al. has explored UV-curable silicone materials with tunable mechanics to allow 3D printing on the basis of developing post-cure mechanical control; nevertheless, their method focuses on UV systems and cannot be easily applied to thermally-curing LSR/TiO_2 composite inks [1]. Young et al. showed gradient stiffness silicone printing of ultrasoft architectures, showing effects of process parameters on mechanical gradients, but not high-permittivity filler incorporation and related dielectric characterization [4]. Davoodi et al. demonstrated high-speed drop-on-demand carbon fiber/silicone sensor printing, which was proven to be high throughput without delving into nanoparticulate dielectric fillers or phase transitions [7]. In a review by Liravi and Toyserkani, additive manufacturing of silicones is summed up, with dispersion and curing as key issues, but requiring systematic research correlating the phases of evolutionary fillers that is the focus of our work [9].

Elizalde-Herrera et al. also assessed graphene as a kind of composite and explained filler-matrix interactions to be exploited in functional properties, highlighting the importance of assessing the evolution of the phase of dielectric fillers when embedded within elastomer matrices [10]. Nieva-Esteve et al. prepare tunable viscoelastic silicone gel inks and showed to be able to carefully tune polymer additive interactions to achieve discrete DIW printability, although the effect of crystalline phasing of inorganic fillers was not given as much attention [11]. Yang et al. have described DIW of functional composites that makes use of supramolecular interactions; the article demonstrates a high level of bonding motif control, although it does not provide a combined spectroscopic/crystallographic correlation to the fillers, which are inorganic nanoparticles [12].

Rius-Bartra et al. investigated high-consistency silicone rubbers with tuned modulus; data show results of industrially relevant formulations, but do not include results of combined microscale dispersion studies with DIW rheology [16]. Duran et al. surveyed silicone and polyurethane elastomers as medical devices; and noted the trade-off between mechanical reinforcement and printability at increased filler loadings; but extensive FTIR rheology databases are lacking [20]. Miron et al. further characterized material characteristics of 3D-printed silicones in detail with characterizing microstructure determining mechanical performance; the break comes in correlating nanoparticle crystallography with rheological activity of DIW ink [28]. Altogether, these recent investigations show progress in silicone ink development, rumor elastic control and DIW parameter control, but little literature describes an entirely linked dataset, which jointly relates FTIR (chemical interactions), XRD (anatase/rutile development) SEM (dispersion/agglomeration), and rheology (shear-thinning, viscosity dynamics) along with the practical DIW printability and part performance [9]-[13], [16], [20], [28].

Recent works by Palanisamy et al. [41] and few others have advanced bio- and fiber-based composites by improving filler–matrix interactions and mechanical stability. Palanisamy et al. [41] demonstrated strong interfacial bonding in natural fibers, while their review [42] emphasized dispersion challenges in bio-derived matrices. Padmanabhan et al. [43] and Aruchamy et al. [44] optimized hybrid stacking for strength enhancement, whereas Ayrilmis et al. [45] and Ramasubbu et al. [46] highlighted the influence of filler morphology and surface chemistry. However, these studies largely focused on organic reinforcements. The present research uniquely incorporates rutile TiO_2 nanoparticles into LSR, addressing dispersion, rheology, and print fidelity through integrated multi-characterization.

Key findings of comparative analysis of recent existing research based on this research analysis is following in Table 1 with comparison with this research work.

Table 1. Comparison of DIW-Based Silicone Composite ink, Characterization and Additives

No.	Reference (Author, References)	Publication Year	Additive Used	Rheology (viscosity)	FTIR	XRD (phase)	SEM / Dispersion	DIW printability / process
1	Foerster et al., [1]	2021	UV-curable silicone matrix	✓	✓	✗	✗	✗
2	Nieva-Esteve et al., [11]	2024	Silicone–polymer composite	✓	✓	✗	✓	✓
3	Yang et al., [12]	2021	Supramolecular polymer networks	✓	✓	✗	✓	✓
4	Young et al., [4]	2024	Gradient-modified silicone elastomer	✓	✗	✗	✓	✓
5	Rius-Bartra et al., [16]	2023	High-consistency silicone rubber	✓	✗	✗	✓	✗
6	Liravi & Toyserkani, [9]	2018	Pure silicone systems (review)	✓	✗	✗	✓	✗
7	Duran et al., [20]	2023	Polyurethane–silicone blend	✓	✓	✗	✓	✗
8	Davoodi et al., [7]	2020	Carbon-fiber reinforced silicone	✓	✗	✗	✓	✓
9	Miron et al., [28]	2021	Silicone-based elastomer composites	✓	✓	✗	✓	✗
10	Elizalde-Herrera et al., [10]	2024	Graphene–silicone composites	✗	✓	✗	✓	✗
11	*This Research Work*	*2025*	*TiO_2*	✓	✓	✓	✓	✓

As highlighted in Table 1, previous DIW studies on silicone-based composites have primarily explored diverse filler systems—such as carbon-based, polymeric, graphene, or supramolecular structures—each offering distinct functionalities but rarely addressing inorganic oxides like TiO_2 within liquid silicone matrices. These earlier studies [1], [4], [7], [9]-[12], [16], [20], [28] were limited by partial or fragmented characterization approaches, often analyzing either rheology or morphology in isolation, without integrating chemical, structural, and printing performance evaluations. None conducted a full-spectrum characterization combining FTIR, XRD, SEM, rheology, and DIW process validation within a unified framework. In contrast, the present research systematically incorporates TiO_2 nanoparticles into LSR to establish a holistic structure–property–process correlation, encompassing chemical bonding (FTIR), phase/crystallinity evolution (XRD), microstructural dispersion (SEM), rheological behavior (viscosity analysis), and DIW printability. The study aims (1) to develop a family of LSR/TiO_2 inks with controlled filler concentrations; (2) to analyze cross-linked interactions through integrated FTIR/XRD/SEM/rheology methods; and (3) to identify an optimized formulation and printing window ensuring maximum dispersion, mechanical reinforcement, and dimensional fidelity. This comprehensive approach directly addresses the limitations of earlier DIW investigations and bridges the methodological and functional gaps in silicone-based composite research.

MATERIALS AND METHODS

Materials Selection

In this research, the primary materials used for composite ink formulation were Liquid Silicone Rubber (LSR), Titanium Dioxide (TiO_2) nanoparticles, glycerol, and a curing catalyst. The LSR system (Grade: LSR-220) is a two-part liquid silicone rubber comprising a base compound (Part A) and a curing agent (Part B). Part A is a milky-white, low-viscosity liquid, while Part B is a light-yellow liquid that initiates the crosslinking reaction upon mixing, transforming the blend into a solid elastomer. The material was procured from *Jay Enterprises Specialty Chemicals (India)* and was selected for its superior elasticity, chemical inertness, thermal stability, and proven processability in Direct Ink Writing (DIW) and soft-device manufacturing [13]-[15]. The inorganic filler, Titanium Dioxide (TiO_2), with the chemical composition TiO_2 (one titanium atom bonded to two oxygen atoms), was employed as the reinforcing additive. A rutile-grade TiO_2 nanopowder with an average particle size of ≈100 nm (uncoated) was obtained from *Padmanathi Distributors (India)*. TiO_2 loadings of 0, 5, 10, and 15 wt% were selected to examine the effect of filler concentration on mechanical reinforcement, dielectric strength, and interfacial bonding within the silicone matrix [16]-[18].

Glycerol (gel form), supplied by *RK World Infocom Pvt Ltd.*, acted as a rheological modifier and dispersing aid, enhancing viscosity control and preventing nanoparticle agglomeration during mixing and extrusion [19], [20]. The curing catalyst (LSR-2 Series, CAF-2) facilitated uniform crosslinking of the LSR polymer chains, ensuring stable network formation throughout the DIW process [18]. Altogether, the chosen constituents exhibited excellent compatibility for DIW-based additive manufacturing, enabling the fabrication of mechanically reinforced, flexible LSR/TiO_2 composites with controlled rheology and curing characteristics suited for next-generation dielectric, soft-robotic, and biomedical applications [21]-[25].

Ink Formulation

The preparation of composite inks including LSR, TiO_2 nanoparticles, catalyst, and glycerol was done as a part of formulation as illustrated in Figure 1. The inks were to have optimum rheological properties, printability and integrity. The mass percentage of each component was obtained by standard equation of mass percentage:

$$wt\% = \frac{Component\ Mass}{Total\ mass} \times 100 \quad (1)$$

where:

1. Component Mass refers to the amount of LSR, TiO_2, Catalyst, or Glycerol.
2. Total Mass = $LSR + TiO_2 + Catalyst + Glycerol$

Table 2 summarizes the resulting formulations of four different ink compositions (DI-I to DI-IV). All compositions contain a fixed base of LSR and catalyst, and TiO_2 contents (0 -15 wt) and glycerol were increased in one proportional manner to achieve equal total mass and printable viscosity.

Table 2 compositions show a systematic change in TiO_2 and glycerol concentration. As TiO_2 loading was increased, the glycerol content was varied to maintain the optimal flow characteristics and dispersion. A magnetic stirrer with borosilicate beakers and glass beads was used to mix with the mixture maintaining speeds of between 20 to 200 RPM. The overall mixing time was range of

Table 2. Formulation Composition and Weight Percentages of LSR/TiO_2 Inks

Composition No.	LSR (wt %)	TiO_2 (wt %)	Catalyst (wt %)	Glycerol (wt %)
1	84	0	1	15
2	73	5	2	20
3	62	10	3	25
4	51	15	4	30

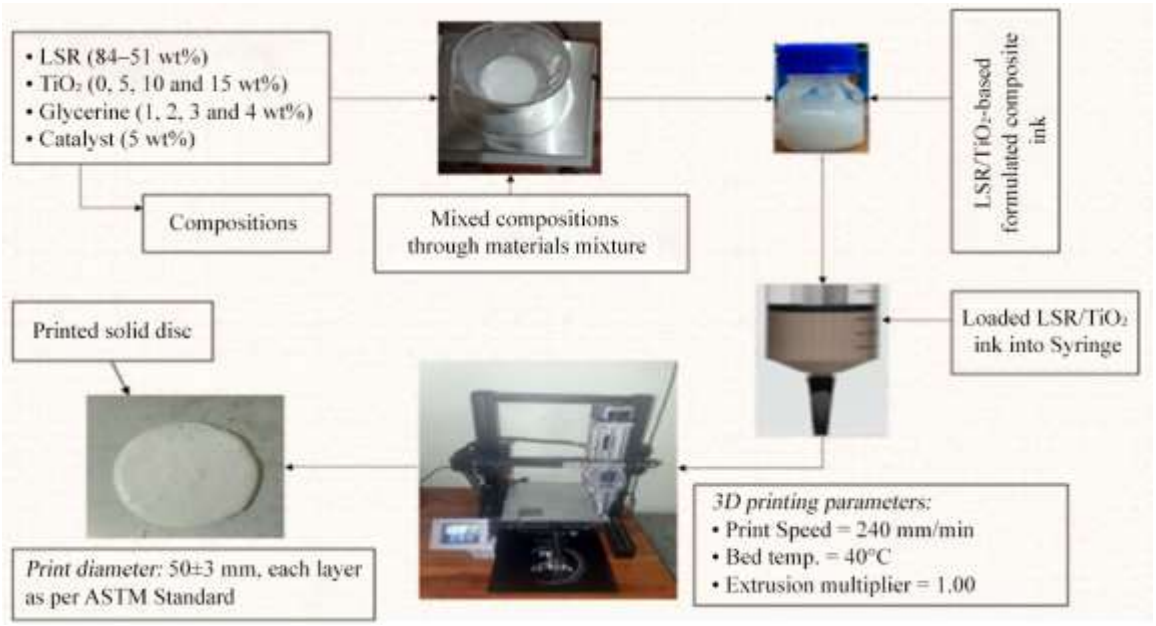

Figure 1. Process Flow for the Formulation and 3D Printing of LSR/TiO_2 Composite Inks

30 minutes to 75 minutes in relation to TiO_2 content and the higher the content the longer the period was taken in the homogenization process. The composite inks were then vacuum degassed to get rid of the trapped air and thus a bubble-free extrusion. All the formulations were prepared at ambient temperature and this is to guarantee consistency in the rheological behavior and the curing kinetics [16] - [19].

The obtained LSR/TiO_2 inks were DIW printed in syringes by keeping the extrusion pressure constant at 2n and the bed temperature constant at 0.13 and reported in the following section. The systematic workflow/process formulation is illustrated in Figure 1. The resultant LSR/TiO_2 inks were DIW printed in syringes under conditions of constant extrusion pressure and controlled bed temperature, as indicated in the following section. The systematic workflow/process formulation is illustrated in Figure 1.

Figure 1 illustrates the consecutive procedure of fabrication of TiO_2 reinforced LSR composite inks. The process starts with the proper quantity of ingredients- LSR (84 - 51 wt%), TiO_2, (0 - 15 wt%), glycerol (1 - 4 wt%), and catalyst (5 wt%) and combine them thoroughly by a mechanical stirrer to bring about homogeneity. The resulting slurry was vacuum-degassed and transferred into a DIW syringe system into which to undergo extrusion. The printing was carried out at 240 to 540 mm/min speed, 40 to 80 ℃ bed temperature, and extrusion multiplier = 1.00 with printouts of circular discs of 50 mm x 3 mm in solid form, which met the ASTM152 standard. Figure 1 is used to successfully follow the logic of the workflow between the compositional design and material integration to the actual fabrication of printed specimens that prove the reproducibility and scalability of the LSR/TiO_2 ink formulation protocol [20]-[22].

Methods

A suite of advanced characterization techniques was utilized in an effort to analyze and assess the performance, compatibility and printability of the developed LSR/TiO_2 composite inks. Rheological characteristics, i.e. viscosity and shear-thinning behavior, were determined using a Labman LMVD-200 rotational viscometer, where the conditions of stability in all flow characteristics were ensured to direct Ink Writing (DIW) applications [26]-[28]. The chemical bonding and molecular interactions of LSR-TiO_2-Glycerol were studied by Fourier Transform Infrared Spectroscopy (FTIR) with FTIR Spectrometer that indicated crosslinking and compatibility of the components were achieved [29], [30].

An X-ray Diffractometer (XRD) was used to determine the crystalline structure and phase distribution of TiO_2 in the cured silicone matrix and found that the phase retention and incongruous dispersal of fillers had been achieved [31]. The morphology of the surface, filler distribution, and bonding in the interface of the composite were examined using Field Emission Scanning Electron Microscopy (FE-SEM) combined with an Energy Dispersive X- ray Spectroscopy (EDS) attachment (JEOL JSM-7610F Plus, EDS: OXFORD EDS LN 2- free, Au Coater: JEOL Smart Coater) [32]-[35]. The combination of these complementary methods gave a comprehensive view of physicochemical and structural properties of the ink making a direct linkage between the formulation design and the Fidelity of DIW print [38]-[40].

3D Printing Process

To provide visual clarity of the experimental system used for Direct Ink Writing (DIW), Figure 2 presents the schematic representation of the DIW machine. The labeled parts illustrate the key functional components involved in the extrusion-based 3D printing of LSR/TiO_2 inks. Figure 2 shows the key elements of a typical direct ink writing (DIW) 3D printing system organised and labelled respectively as a to i. The fabricated part (a) is the resultant last structure, which is developed layer by layer as the material is carefully extruded on the surface. The manual control unit (b) enables the operator to manipulate and adjust printing parameters manually, which makes the printing process controlled in real time. The key element in the deposition system is the nozzle (c), in which the ink is extruded using high precision.

The syringe casing (d) fixed the ink syringe in place during working and made it stable and aligned. Above this, the extrusion motor (e) operates the mechanical power needed to rotate the extrusion screw (f), pushing the ink down through the nozzle. The print bed (g) is a stable work table that the part rests on as the material is deposited on it. Controlled movement within the horizontal plane is achieved through the use of the X-Y platform (h), where the nozzle or the print bed could be moved appropriately to outline the shape of the constructed print through the geometry. Lastly, the ink

Figure 2. Illustration of DIW based 3D printer, (a) Part Fabrication, (b) Manual Control Unit, (c) Nozzle, (d) Syringe Casing, (e) Extrusion Motor, (f) Extrusion Screw, (g) Print Bed, (h) X-Y Platform, (i) Ink Syringe, (j) Print Head

syringe (i) holds the viscous ink to be used in the manufacturing process and injects it into the extrusion screw, which allows for accurate deposition. Such a direct system allows producing high-resolution prints using paste-like materials of complex geometries [36], [37].

RESULTS AND DISCUSSION

The experimental results of LSR/TiO_2 composite inks are initially examined in detail, such as measurements of viscosity, chemical interaction, crystallinity and microstructure. To evaluate the rheological behavior of the inks their shear-thinning properties (in essence properties of the inks for Direct Ink Writing (DIW) applications) were measured. Chemical interactions and the phase composition were studied using Fourier Transform Infrared Spectroscopy (FTIR) and X-ray Diffraction (XRD). Insights on dispersion of TiO2 in polymer matrix were gained via Scanning Electron Microscopy (SEM). Tables and figures aid correlation of formulation parameters with structural, mechanical and printability properties of the material in this work.

In this research work, Labman LMDV-200 viscometer was used to analyze the viscosity of LSR/TiO_2 inks at controlled temperature of 19.1°C and spindle L4 at 10 RPM. The results obtained for the viscosity with various ink formulations showed the shear thinning behavior present in case of direct ink writing (DIW) applications.

Figure 3 and corresponding Table 3 show the change of dielectric ink viscosity of four DIW samples (DI-i to DI-iv) when the shear rate (10 RPM) is kept constant. Each of our sample's maximum viscosity in this analysis we taking in terms of its trail, In DI-i (0% TiO_2), identity of viscosity is 27,118 mpa.s. On incorporation of 5% TiO_2 in DI-ii, viscosity rises drastically to 29,795 mpa.s, which means that the particle/matrix interacts firmly. Nonetheless, when TiO_2 is again increased to 10 % (DI-iii) and 15 % (DI-iv), viscosities of 24,868 mpa.s and 29,162 mpa.s are obtained respectively. The implication of this trend is that excess filler can interrupt the uniformity of dispersion or cause the agglomeration of particles, scaled down resistance to the flow. This non-linear viscosity behavior is confirmed graphically by Figure 3.

Table 3. Viscosity Measurements of LSR/TiO_2 Inks.

Sample No	R.P.M.	Viscosity (mPa·s)
DI-i	10	25321
		26912
		24662
		27118
		27043
DI-ii	10	27940
		28432
		25414
		29795
		27781
DI-iii	10	23485
		24868
		22752
		22543
		22310
DI-iv	10	27852
		26132
		25181
		29162
		27690

Note DI-i to DI-iv is the Dielectric ink sample I to IV*

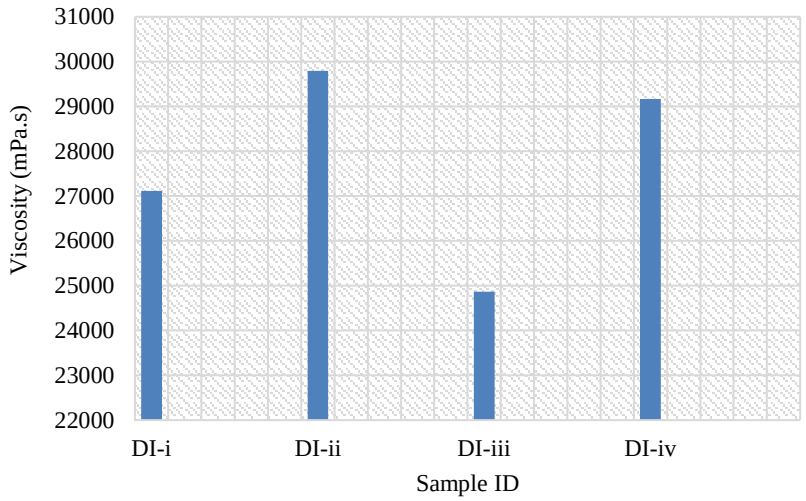

Figure 3. Viscosity measurements of LSR/TiO2 dielectric Ink Samples

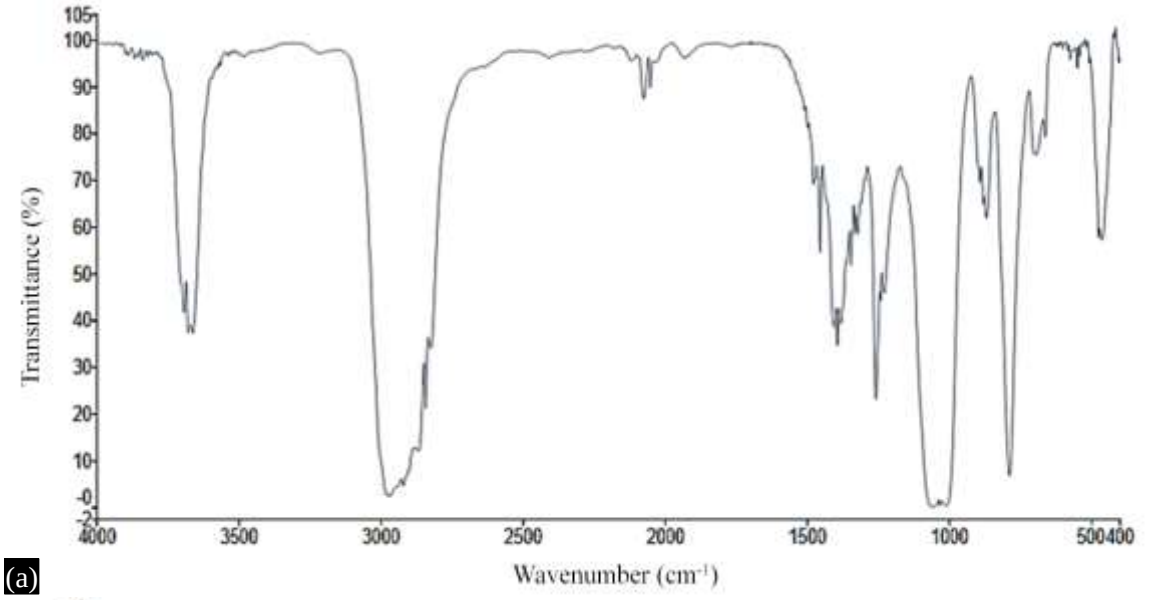

(a)

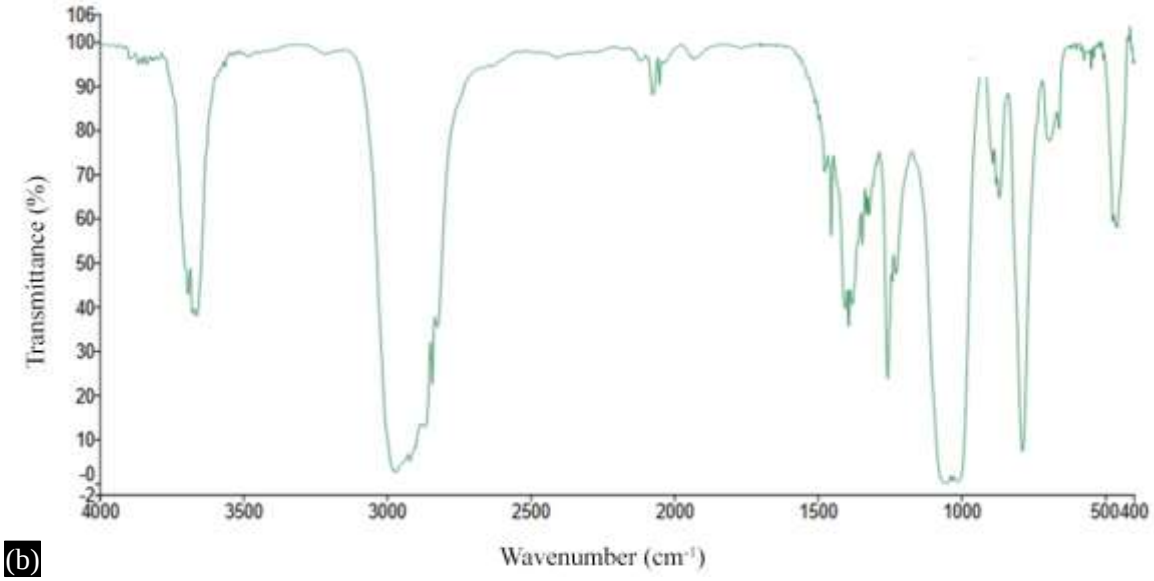

(b)

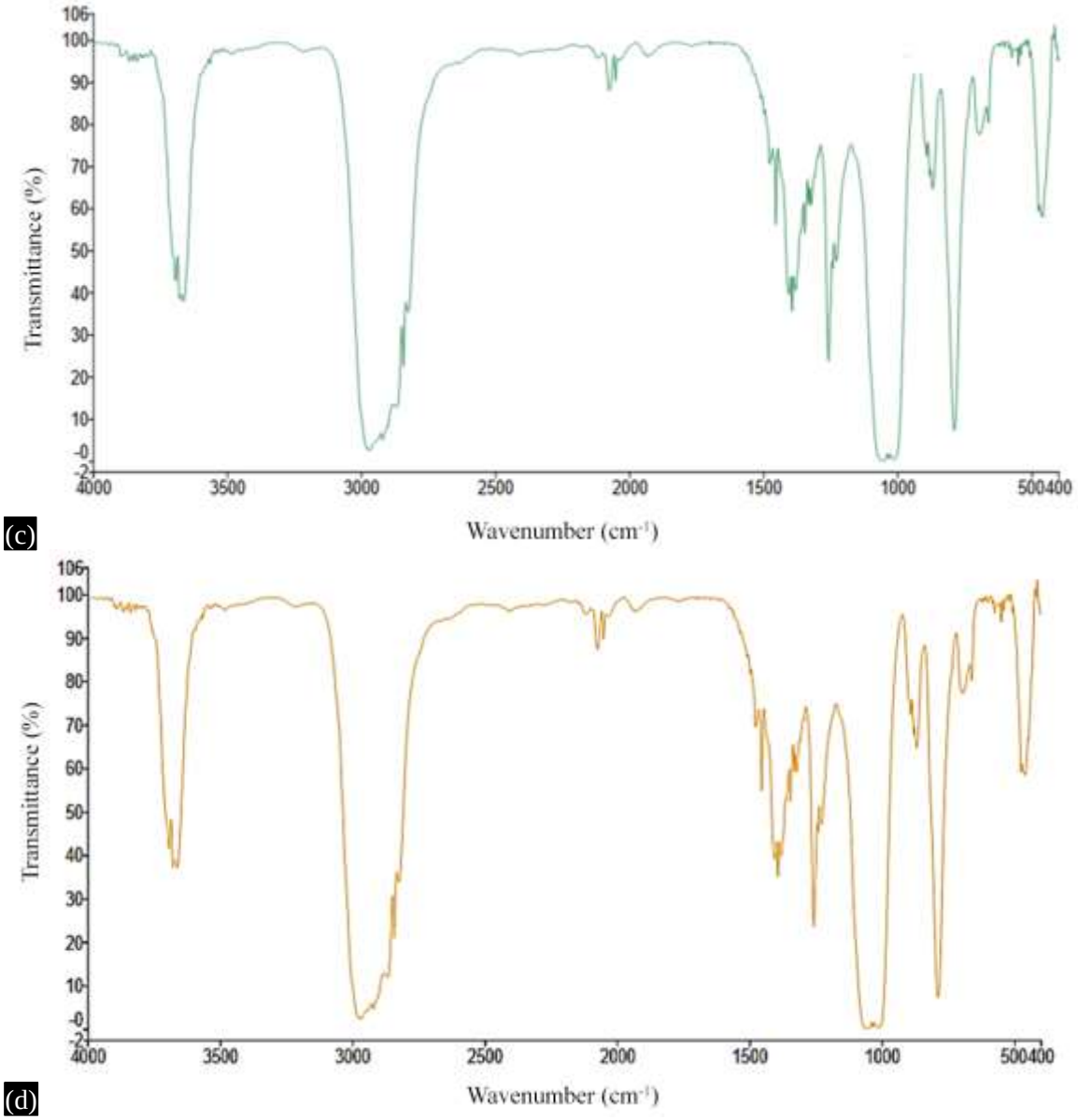

Figure 4. FTIR Spectra of LSR/TiO_2 Composites, (a) Pure LSR Spectrum, (b) LSR with 5 wt% TiO_2, (c) LSR with 10 wt% TiO_2 and (d) LSR with 15 wt% TiO_2

The detected viscosity trend of each of the sample's DI-i up to DI-iv is a product of interaction among filler content of TiO_2 and level of polymer matrix. First, in DI-ii (5% TiO_2), the viscosity increases because TiO_2 nanoparticles are homogeneously distributed, thereby strengthening intermolecular interactions and raising the flow resistance. With increased concentrations (10% and 15% TiO_2 in DI-iii and DI-iv), however, the viscosity goes down. This decrease is attributed probably to particle agglomeration, and heterogeneous dispersion, which results in microstructural interstices or less effective surface contact of particles with the matrix. These effects degrade the rheological structure and, thus, reduce the overall viscosity.

Figure 4(a)–(d) represents the FTIR of LSR/TiO_2 composites with different TiO_2 loading: (a) pure LSR, (b) 5 wt% TiO_2, (c) 10 wt% TiO_2, and (d) 15 wt% TiO_2. In all four spectra, distinct peaks of the silicone bound are regularly found, i.e., Si-O-Si stretching (~1000 - 1100 cm^{-1}), Si-CH_3 bending (~1250 cm^{-1}), and broad -OH starching (~ 3300 cm^{-1}), which also indicates that the silicone structure is stable even in the presence of TiO_2.

With increasing TiO_2 concentration, additional absorption bands of the lower wavenumber (~500 to 650 cm^{-1}) grow stronger, which is attributed to Ti-O-Ti stretching vibrations. These bands are observed in faint form when spectrum (b) is analyzed and getting stronger when analyzing spectrum (c) and (d), and these bands testify to physical integration of TiO_2 nanoparticles into the LSR matrix. Importantly, no new peaks or significant shifts are observed in the main functional group regions of LSR, suggesting the absence of chemical interaction between TiO_2 and the polymer chains. This indicates that the interaction is purely physical, and the silicone backbone remains unaffected. The differences among the spectra are thus primarily due to the increasing intensity of TiO_2-related peaks, not due to any transformation of the silicone's chemical structure.

This research study looked at the crystal structure and phase makeup of TiO_2-reinforced LSR-based inks using XRD analysis. Figure 5(a)–(d) displays the XRD patterns of the pure base LSR formulation combined with different amounts of TiO_2 reinforcement (5 wt%, 10 wt%, and 15 wt%).

Figure 5(a) displays the base LSR ink's amorphous silicon network that produces a wide and weak hump centered between 22° and 25° 2θ. XRD analysis shows diffraction peaks that are absent, which confirms the LSR/catalyst/glycerol matrix exists either as nanocrystalline or amorphous structures. The XRD pattern in Figure 5(b) shows four ordered peaks that match up with the anatase phase of TiO_2 at 2θ values of 25.3°, 37.8°, 48.0°, and 55.1°. The observed patterns indicate the simultaneous development of crystallites while the polymer interacts with the filler.

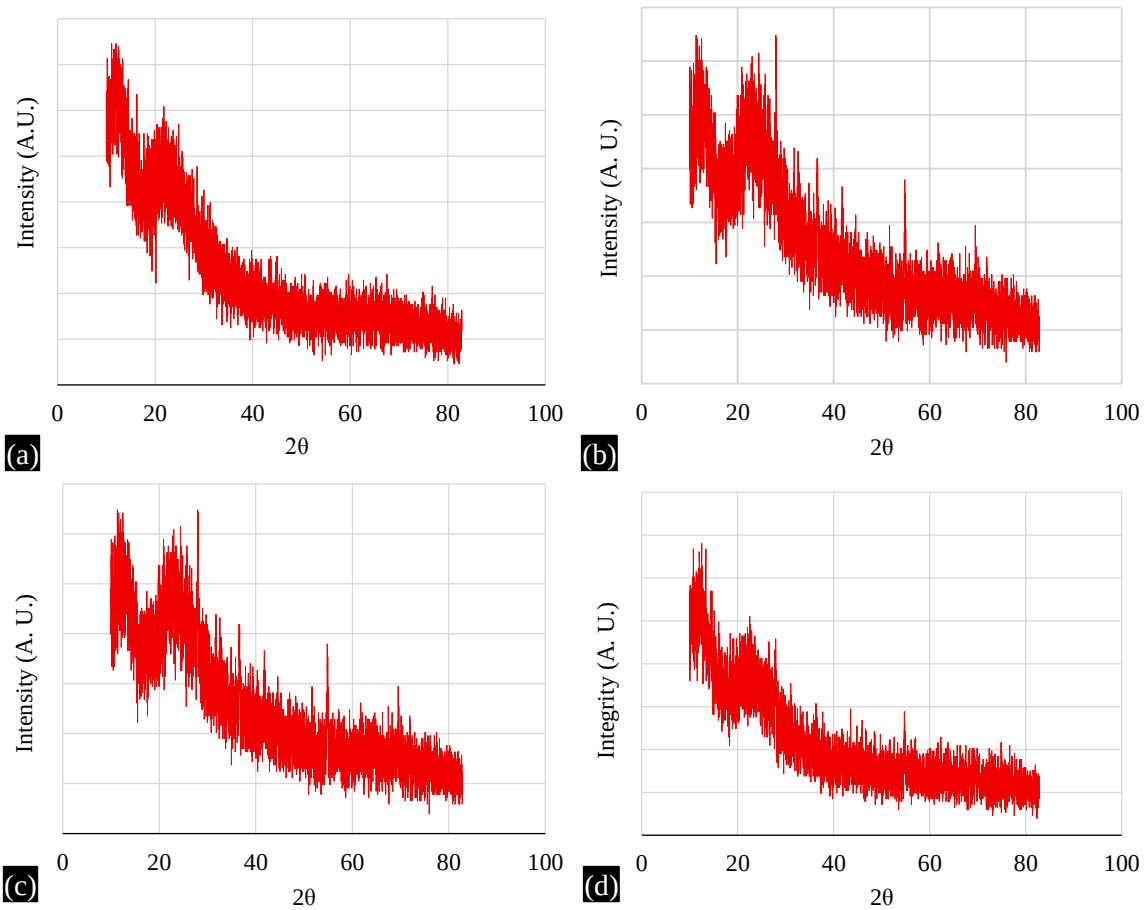

Figure 5. XRD Patterns of LSR/TiO_2 Composites, (a) XRD pattern of pure LSR, (b) XRD pattern of LSR with 5 wt% TiO_2, (c) XRD pattern of LSR with 10 wt% TiO_2, (d) XRD pattern of LSR with 15 wt% TiO_2

Figure 5(c) demonstrates that the TiO_2 anatase X-ray peaks were sharper and stronger because of the better filler distribution and stronger bonds between the interfaces within the material. Due to these changes in organs, rheological stability is increased. Incorporation of 15 wt%. TiO_2 in Figure 5(d) leads to intensification of the anatase peaks accompanied with the emergence of new reflections at 27.4°, 36.1°, and 41.2° due to the formation of the new rutile TiO_2 phase. This metamorphosis foreshadows higher crystallinity, which enhances mechanical strength and increase thermal resistance in addition to undesirable printability Behaviour due to potential material aspect rigidity and agglomeration complications. The development of XRD pattern with loading to TiO_2 exhibits the effective loading of nanoparticles and indicates a structural correlation which influences mechanical printability in the composite ink series. LSR/TiO_2 composites can be used in Direct Ink Writing applications, since they possess appealing crystalline properties.

SEM micrographs of Sample 1 (Figure 6(a)–(f)) display the natural surface morphology of pure Liquid Silicone Rubber (LSR) without TiO_2 reinforcement. The surface of the samples as shown in Figure 6(a)–(c) is smooth and homogenous with microvoids that are well dispersed as a result of inherent crosslinking of polymer and the release of gases during curing. The fact that there are no particulate characteristics shows that the LSR matrix is structural uniform with well-developed polymer chains and no defect inside a crosslinked network. The observed spherical voids at increased magnifications are explained by entrapment of low-volatilities that are emitted in the course of the cure, which is common in untouched silicone systems. All these characteristics signify a wonderful level of polymer homogeneity, which demonstrates the effective curing and the performance of the silicone structure.

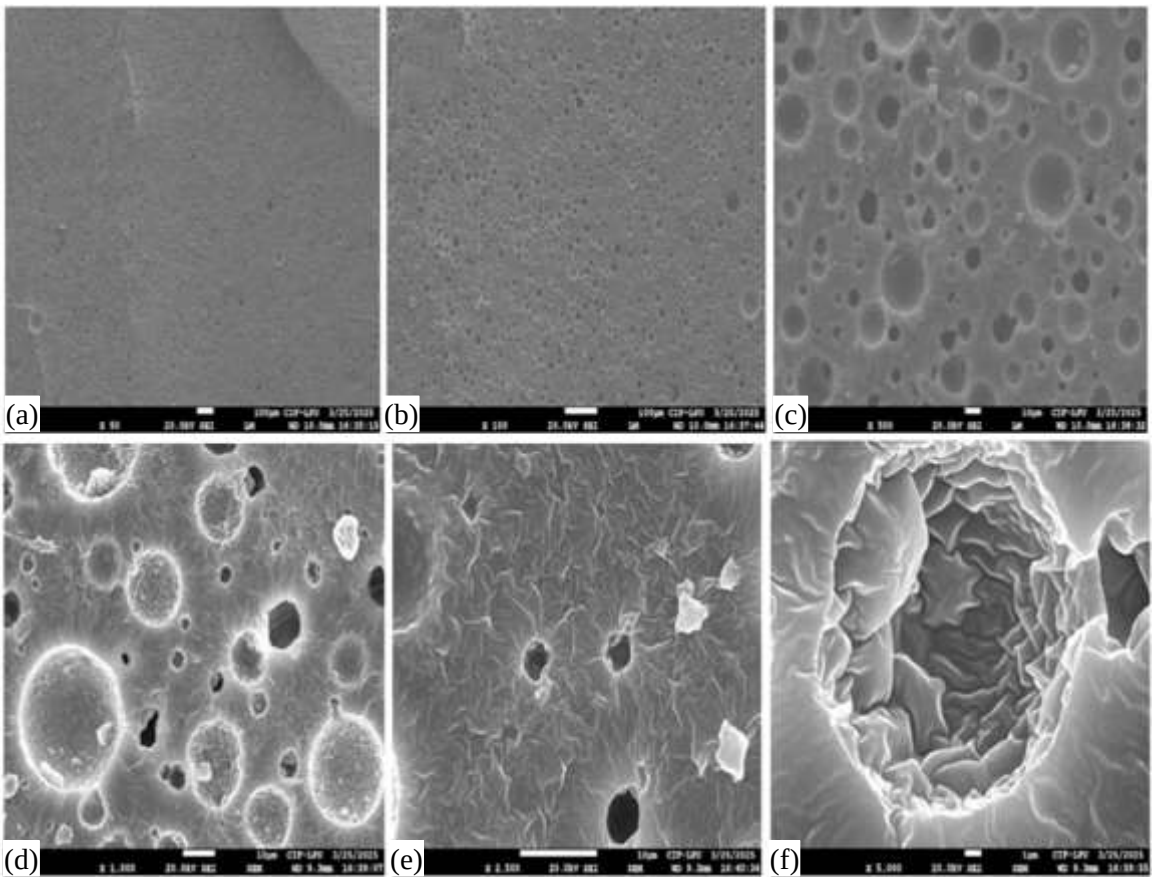

Figure 6. (a)–(f) SEM micrographs of Sample 1 – Pure LSR (0 wt% TiO_2) at varying magnifications showing (a)–(c) uniform surface morphology with microvoids, and (d)–(f) high-magnification views revealing a dense, defect-free silicone matrix prior to TiO_2 addition

In increased magnifications (Figure 6(d)–(f)), the surface of the matrix shows a uniform topography with few microcracks or phase boundaries, which prove the elasticity and stability of the pure LSR film. The low-roughness and high-dense network are indicative of high inter-chain bonding and adequate density of crosslinking, which are necessary to ensure that the dimensional accuracy remains accurate during direct ink writing (DIW). The fact that there are no TiO_2 nanoparticles also suggests that the morphology that was observed was exclusively determined by the LSR polymerization and curing mechanisms. This standard morphology plays a very important role in comparative analysis because it gives a standard point of reference when determining how the morphological changes brought about by the addition of the TiO_2 elements to the later samples. Overall, it is clear that the SEM characteristics of Sample 1 (Figure 6(a)–(f)) are sufficient to justify the research background, as the pristine LSR matrix is also uniform, well-cured, and can be further reinforced with nanofillers using DIW composite.

SEM micrographs of Sample 2 (Figure 7(a)–(f)) illustrate the morphology of the LSR matrix based on the addition of 5 wt% TiO_2 nanoparticles. Figure 7(a)–(c) indicates that the surface is significantly more textured but the fine LSR sample, and the energized particles are uniformly distributed in the matrix in the form of fine spheres of TiO_2. In these micrographs, the filler phase is well dispersed and there is a little indication of agglomeration of particles, which indicates that 5 wt% TiO_2 is the optimum content in terms of homogeneous dispersion. The enhanced surface topography and moderate enhancement of roughness both point to effective surface interfacial bonding between the TiO_2 nanoparticles and the LSR matrix. The mechanism behind this interaction is probably a chemical partial affinity of silanol groups of LSR and surface hydroxyl TiO_2 groups, which lead more to the adhesion of the filler and the matrix and the maximized occurrence of mechanical interlocking between the interface.

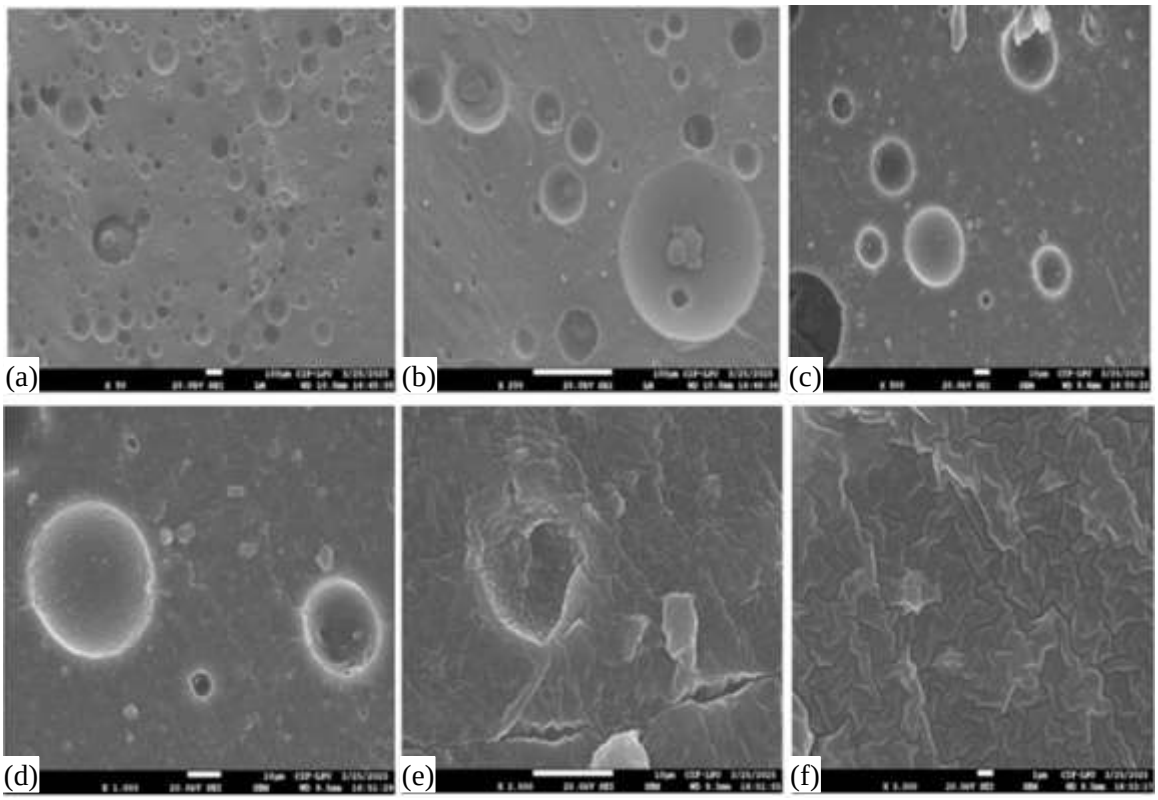

Figure 7. (a)–(f) SEM micrographs of Sample 2 – LSR/TiO_2 (5 wt%) composite at different magnifications showing (a)–(c) uniform spherical dispersion of TiO_2 within the LSR matrix and (d)–(f) high-magnification views illustrating enhanced interfacial bonding and well-cured surface morphology indicative of optimal filler integration.

At increased magnifications (Figure 7(d)-(f)), the particles of TiO_2 are observed to be well encapsulated in the LSR network, creating continuous and stable interfaces. The lack of great voids or cracks implies effective wetting and dispersion in the formulation process of the ink. The microstructure is characterized by fine and wrinkle like texture, which is common to well-cured silicone composites, which in addition, provides dimensional stability and elastic recovery during Direct Ink Writing (DIW). This is by virtue of the fact that this morphology supports that the addition of 5 wt% TiO_2 does not negatively affect the microstructural integrity but does not adversely affect homogeneity, which supports the given formulation strategy, as it has been employed in this study. Therefore, Figure 7(a)–(f) shows that intermediate TiO_2 addition is able to enhance the LSR matrix to make it stronger to achieve better filler-polymer compatibility and printability, and the structural uniformity at the same time, which justifies the compositional methodology of the given study.

SEM micrographs of Sample 3 (Figure 8(a)–(f)) indicate the significant change in surface morphology when loading TiO_2 is increased to 10 wt%. As can be observed in the Figure 8(a)–(c) LSR matrix has become strongly uneven and porous relative to the presence of lower filler concentrations. There are also too many large and irregular voids that can be observed in the microstructure which are a sign of partial filler agglomeration and low dispersion uniformity. The coincidence of TiO_2 particles at local areas indicates that, at a certain critical point, filler interaction will take over the filler matrix bond. This agglomeration inhibits the homogeneity of the silicone network and creates microvoid clusters which can be the stress concentrators. The result validates the hypothesis that the 10 wt% loading exceeds the optimum dispersion threshold at 5 wt%, leading to phase separation propensity, as a result of increased crowding and mobility inhibited by viscosity in the LSR medium.

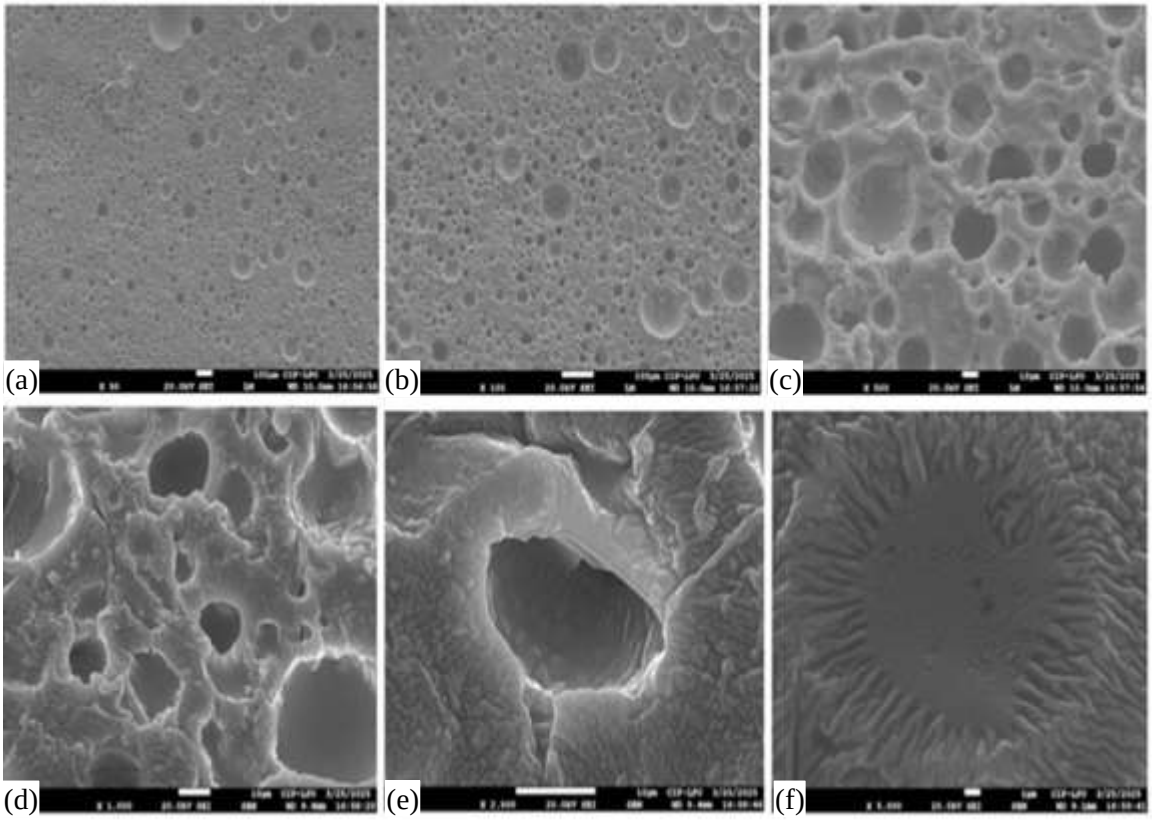

Figure 8. SEM micrographs of Sample 3 – LSR/TiO_2 (10 wt%) composite at varying magnifications showing (a)–(c) roughened, porous surfaces with emerging agglomeration zones and (d)–(f) high magnification images revealing filler clustering, microvoid formation, and disrupted crosslink uniformity at elevated TiO_2 concentration

At increased magnifications (Figure 8(d)–(f)), the TiO_2 clusters become better defined, with the surrounding matrix constriction and microcracks in the periphery suggesting the formation of internal stress during curing. The small and rough topography denotes that the excess to the addition of nanoparticles decreases the flexibility of polymer chains and breaks uniform crosslinking. The cause of this mechanism is due to a lack of polymer encapsulation around TiO_2 agglomerates and restricts interfacial compatibility. The surface morphology therefore confirms the supposition that although TiO_2 increases reinforcement at lower concentrations, high loads impair uniformity and structural integrity of the matrix. Figure 8(a)–(f) thus validates the presence of significant agglomeration and heterogeneity with 10 wt% TiO_2, as well as that the optimum filler concentration of stabilization and printability is below this point- as aligned with the aim of the research: to determine a balance between reinforcement and processability.

SEM micrographs of Sample 4 (Figure 9(a)–(f)) show a largely stabilized but disordered surface morphology at the maximum TiO_2 loading (15 wt). As shown in Figure 9(a)–(c), the presence of large TiO_2 clusters in the composite surface is observed as well as smaller uniformly entrained particles. The level of agglomeration seems to be lower compared to the 10 wt% sample; this could be due to the enhanced redistribution of fillers as a result of the increased system viscosity and mechanical shear used during mixing. This enhanced viscosity must have restricted excessive movement of particles so that components of filler are retained better in the polymeric structure. The micrographs also support the re-establishment of partial homogeneity in which TiO_2 clusters are surrounded by the LSR matrix to create semi-continuous networks that build local reinforcing areas in the composite.

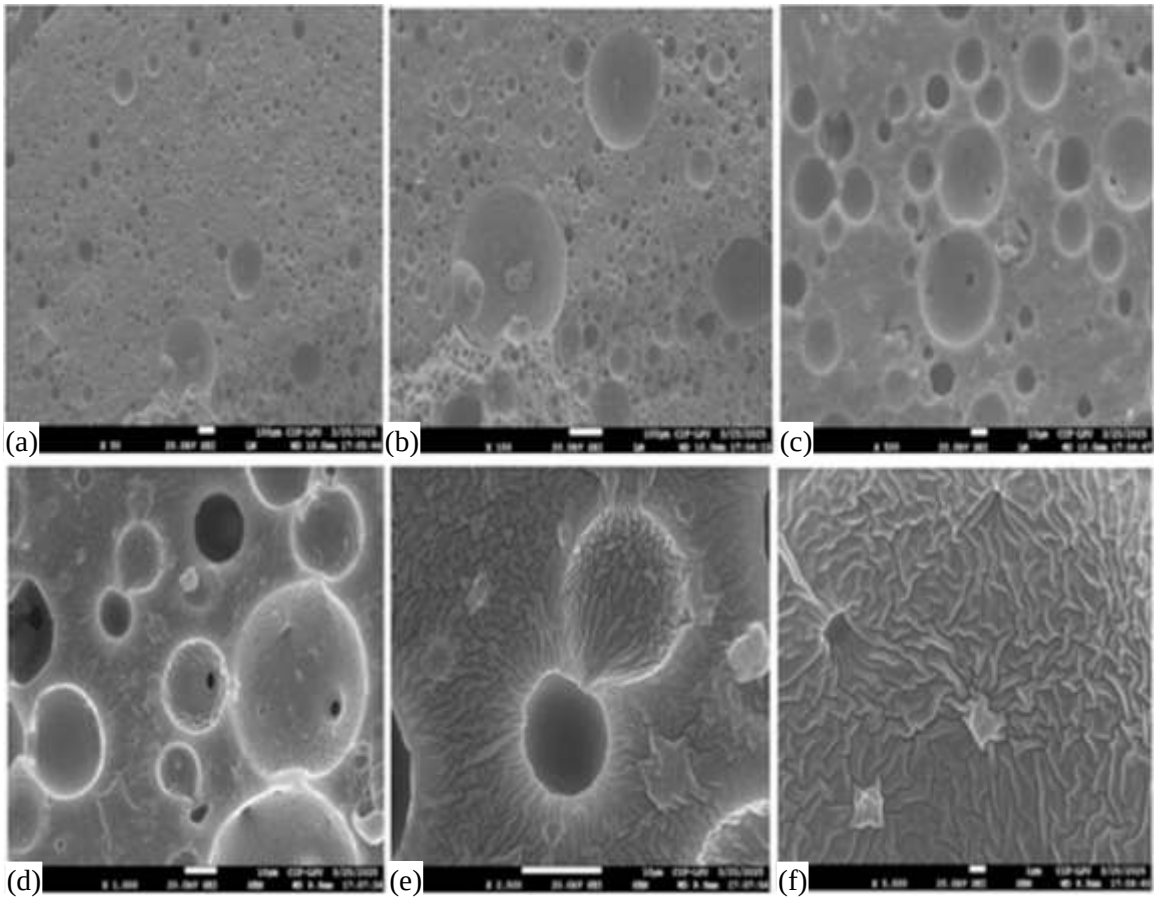

Figure 9. (a)–(f) SEM micrographs of Sample 4 – LSR/TiO_2 (15 wt%) composite at different magnifications showing (a)–(c) redistributed TiO_2 clusters and semi-uniform particle encapsulation within the matrix and (d)–(f) high-magnification views highlighting smoother interfacial transitions, dense cured regions, and viscosity-induced stabilization of filler dispersion

Higher magnifications (Figure 9(d)–(f)) show the LSR matrix more compact, containing fewer open spaces and having a high density of wrinkle-like surface pattern typically of well-cured silicone composites. There are smooth interfacial boundaries of TiO_2 inclusions in the surroundings making the filler-matrix adhesion better than the 10 wt% solution. The morphological study confirms that, although some fraction of TiO_2 is agglomerated, the composite attains a more stable dispersing level under an optimality in shear and curing stipulations. The balance between filler concentration and the flow properties of the matrix is indicated in this result, with an increased viscosity winning over the phase separation. Figure 9(a)–(f) therefore confirms the hypothesis that above 10 wt%, controlled viscosity has the power to counteract agglomeration effects, thus facilitating the research goal of producing rheologically stable and printable LSR/TiO_2 inks that can be used in DIW.

According to the comparative SEM studies of all the four samples, the *Sample 2* (LSR containing 5 wt% TiO_2) formulation features the most optimized microstructure and is thus the best to use in Direct Ink Writing (DIW)-based 3D printing. *Sample 1* contained pure LSR with a smooth and uniform surface and no adequate reinforcement and interfacial stiffness that is essential in ensuring that the structure is not deformed during the extruding process. At wt% TiO_2 (*Sample 3*) a sign of agglomeration, porosity and matrix heterogeneity were observed due to overloading of nanoparticles and therefore, flow uniformity and print accuracy were adversely affected. *Sample 4* at 15 wt% (demonstrating some re-stabilization because of filler redistribution caused by viscosity) although high filler concentration still lowered the elasticity of the matrices and the adhesion of the layers.

The SEM micrographs of the 5 wt% TiO_2–LSR composite revealed a balanced and homogeneous morphology characterized by well-dispersed nanoparticles, strong filler–matrix interfacial bonding, and minimal void content. This uniform dispersion, confirmed through SEM, facilitated the formation of silanol–hydroxyl linkages between TiO_2 particles and the silicone matrix, thereby enhancing cohesive strength and microstructural integrity. Such bonding interactions not only improved rheological consistency—yielding a stable shear-thinning profile—but also translated into superior print fidelity during DIW processing. The homogeneous microstructure ensured smooth material flow, uniform interlayer cohesion, and dimensional stability across printed geometries. Hence, the 5 wt% TiO_2 formulation (Sample 2) was validated as the optimal composition, providing the ideal balance between filler reinforcement, viscosity control, and high-quality part fabrication, thereby establishing a direct correlation between microstructural uniformity and DIW print performance.

Figure 10 shows single-pass rectilinear tracks printed at three sets of parameters (240 mm/min at 40 °C; 390 mm/min at 60 °C and 540 mm/min at 80 °C). At 240 mm/min the filament is continuous though it is somewhat over-extruded which suggests slower shear-induced thinning and increased lateral spreading. The 390 mm/min/60 °C case scores the highest: even strand width, little surface waviness and high substrate adhesion, which is consistent with the speedy post-deposition viscosity recovery, and the average increase in thermal activation of the given curing. With 540 mm/min/80 °C we observe a slight loss of ink and occasional holes, which is evidence of lack of time to consolidate flow; a situation where we can cure more rapidly. Overall, Figure 10 confirms that mid-range speed / temperature optimizes line fidelity of the 5 wt% TiO_2 ink.

In Figure 11, infill boxes (multi-line infill boxes) are printed in the three parameter sets. The 240 mm/min one has strong interstrand bonding and can be noted to have an apparent filament overlap and small end suggest that there are over-deposition and slow curing. The 390 mm/min sample has dense and well-fused infill that has even spacing and low voidage- a sign of proper shear-thinning during extrusion and timely viscosity recovery to allow layer fusion. The infill at 540 mm/min shows minor under-extrusion and lack of full contact between the strands and they result in incomplete fusion in portions; this suggests that high speed negatively affects transfer of materials and curing interaction. Therefore, Figure 11 confirms that 390 mm/min and 60 °C provide the best volumetric filling and strength of the best composite ink.

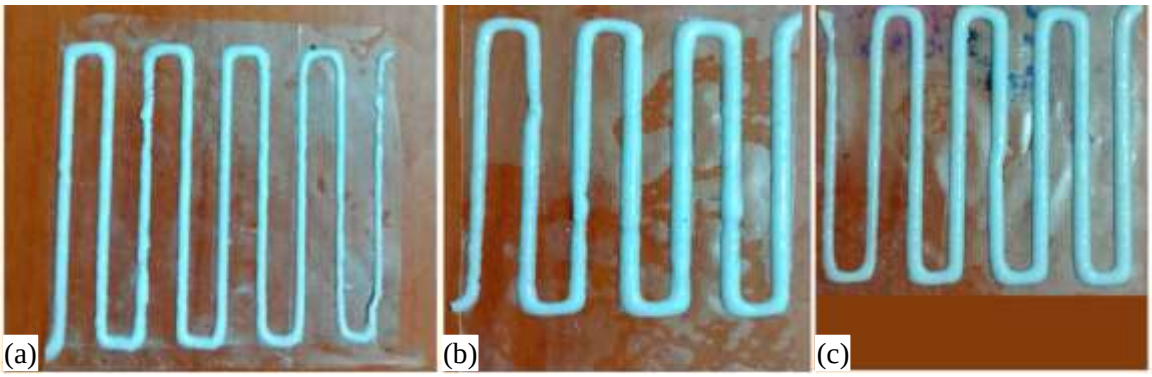

Figure 10. Rectilinear track fabrication of LSR/TiO_2 (5 wt%) composite ink (a) Print Speed 240 mm/min with Temp. 40°C and EM = 1.00, (b) Print Speed 390 mm/min with Temp. 60°C and EM = 1.00, (c) Print Speed 540 mm/min with Temp. 80°C and EM = 1.00

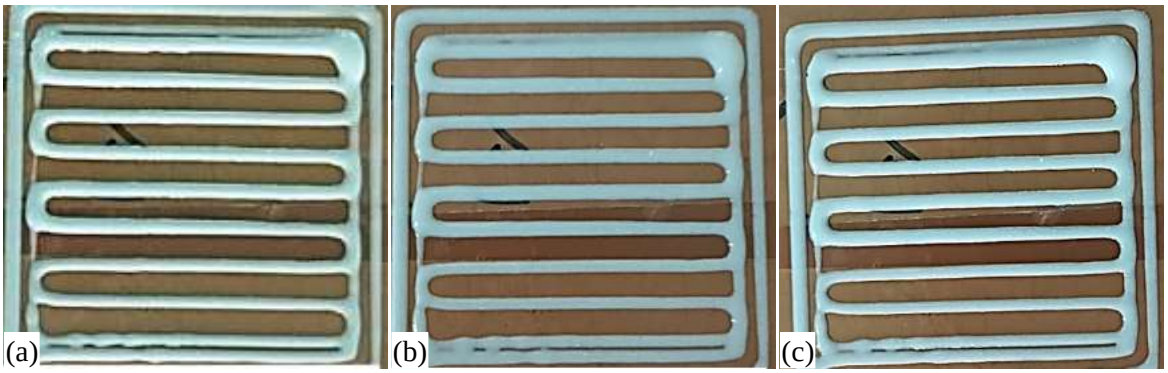

Figure 11. Rectangular infill structures printed using the optimized LSR/TiO_2 (5 wt%) composite ink, (a) Print Speed 240 mm/min with Temp. 40°C and EM = 1.00, (b) Print Speed 390 mm/min with Temp. 60°C and EM = 1.00, (c) Print Speed 540 mm/min with Temp. 80°C and EM = 1.00

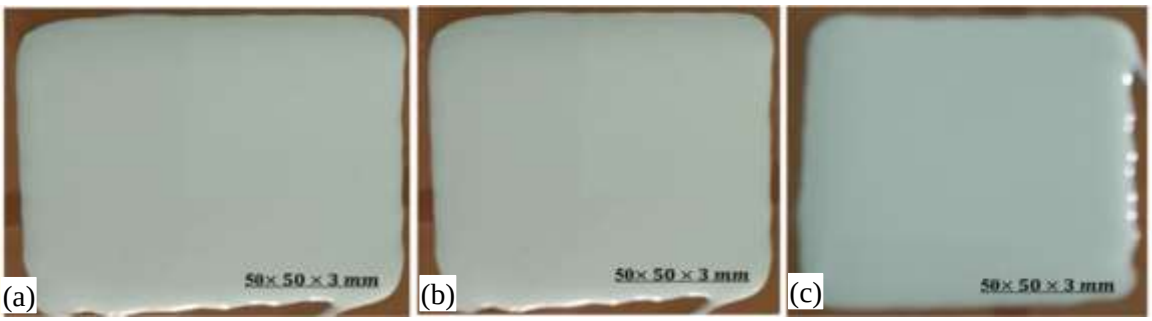

Figure 12. Multi-layer solid sheet fabrication (50 × 50 × 3 mm) of the LSR/TiO_2 (5 wt%) composite ink. (a) Print Speed 240 mm/min with Temp. 40°C and EM = 1.00, (b) Print Speed 390 mm/min with Temp. 60°C and EM = 1.00, (c) Print Speed 540 mm/min with Temp. 80°C and EM = 1.00

Figure 12 represents the structure of multilayer square sheets that are printed under different conditions of 240, 390 and 540 mm/min with substrate temperature of 40, 60 and 80 °C respectively. At speed of 240 mm/min, slight bulging at the edges and surface waviness occurs, which is caused by slower flow and delayed levelling caused by incomplete crosslinking. The sample (390 mm/min, 60 °C) displays a glossy, flawless surface, counterbalanced shear-thinning and rapid viscosity recovery on deposition by well-fused layers. The sheet is continuous at 540 mm/min with a slight decrease in gloss and microvoids which show marginal under-extrusion. The findings prove that 5 wt% TiO_2-LSR ink has a good level of dimensional consistency and interlayer adhesion stability, whereas the 60 °C, 390 mm/min environment gives the sample the best multilayer consolidation.

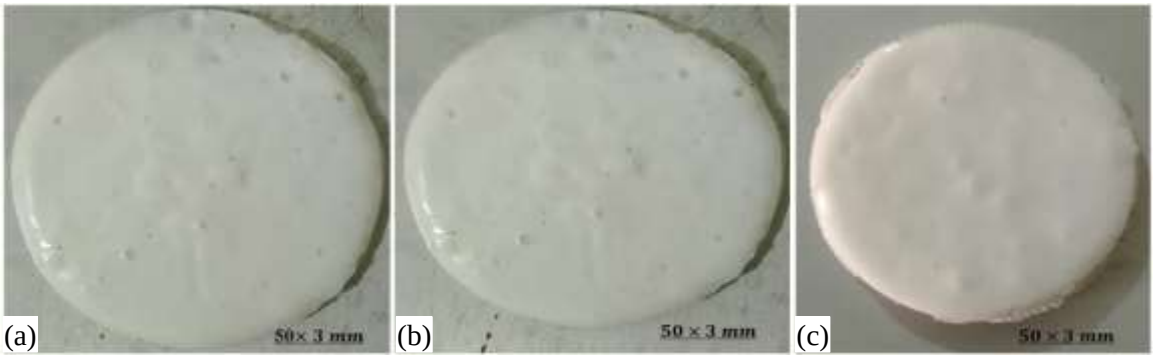

Figure 13. Fabrication of multi-layer solid disc geometries using the LSR/TiO_2 (5 wt%) composite ink (a) Print Speed 240 mm/min with Temp. 40 °C and EM = 1.00, (b) Print Speed 240 mm/min with Temp. 40 °C and EM = 1.00, (c) Print Speed 240 mm/min with Temp. 40 °C and EM = 1.00

In Figure 13, multi-layer solid discs were made at a fixed extrusion multiplier and under different thermal conditions. The printed sample at 40 °C has minor surface porosity, indicating an unfinished curing of the sample and volatiles trapped inside. The most homogeneous texture, circular accuracy and homogenous gloss are observed in the 60 °C disc which is a clear indication of the effective layer bonding and enhanced crosslink density in the LSR/TiO_2 matrix. On the other hand, the 80 °C sample exhibits slight contraction and local warping that could be due to faster crosslinking and thermal contraction. Combined, Figure 13 confirms the existence of moderate thermal energy promoting optimal polymer chain rearrangement and TiO_2 dispersion, resulting in defect-free geometries to use in DIW-based elastomeric printing applications.

The Direct Ink Writing (DIW) experiments which were carried out by using the optimize TiO_2 – LSR composite ink 5 wt% ink showed that there was high stability of the material with no reproducibility in terms of extrusion of any variations in different geometries. Figures 10 and 11 indicate that the print quality and dimensional fidelity change considerably with changing the speed of printing (240 to 540 mm/min) and the substrate temperature (40 °C to 80 °C). The filaments exhibited slight over-extrusion and irregularities at lower speeds and lower temperatures due to delayed recovery of viscosity and incompleteness of curing. On the other hand, very high speeds and temperatures caused thinning, formation of voids and localized contraction with rapid crosslinking. The middle states of 390 mm/min at 60 °C gave the most consistent features have sharp edges, smooth infill and defect-free multilayer structures as reflecting the optimum balance between shear-thinning flow during extrusion and elastic recovery after deposition.

Overall, the printed geometries (rectilinear tracks, infill patterns, multi-stratum layer sheets, and solid discs) confirmed rheological and thermal compatibility of the designed LSR/TiO_2 composite ink of DIW. The TiO_2 nanoparticles improved the interfacial bonding and microstructural reinforcement whereas glycerol controlled the viscosity to ensure uniformity in the deposition of the layers. The dimensional stability and interlayer adhesion as well as the low levels of surface defects involved during optimization of the printing parameter verified that the ink was suitable to be utilized in the manufacturing of high-fidelity elastomeric parts. These outcomes together demonstrate that an intermediate range of temperatures-speed (around 60 °C, 390 mm/min) yields the best print behavior, balancing rheological adjustment tolerance with functional resolution a development superior to the traditional silicone based DIW systems.

As compared to the prior research conducted by Foerster et al. [1], Nieva-Esteve et al. [11], Yang et al. [12], and Duran et al. [19], which focused on printability or rheology of silicone-based and polymeric inks, only, this paper produces a synthesis of FTIR, XRD, SEM, and rheology under a unified characterization paradigm. Past studies had either structural or rheological understanding but

had not been fully validated by full spectrum of filler-matrix interaction. The optimized 5 wt% LSR/TiO_2 composite ink herein formed has a uniform dispersion, controlled viscosity, and improvement in interfacial bonding and overcame agglomeration and print distortions observed in previous reports. The composite runs at 390 mm/min and 60 °C to assure high standards of dimensional accuracy, confirming thermo-rheological optimization beyond current DIW materials on reproducibility and readiness to use.

CONCLUSION

The developed LSR/TiO_2 composite inks showed a high formulation stability and rheological modulation that can be conveniently induced with DIW-based additive manufacturing. The optimal mixture with 5 wt% TiO_2 and regulated glycerol concentration had perfect viscosity and shear-thinning behavior, which ensured consistent extrusion and fast healing after deposition. Effective chemical bonding and crosslinking of LSR and TiO_2 was confirmed by FTIR analysis and XRD analysis proved the presence of TiO_2 crystalline phases that are uniformly distributed throughout the polymer. The homogeneous filler separation was confirmed by SEM micrographs, which also indicated high levels of interfacial bonding and formation of a strong microstructure that is essential toward print stability and mechanical stability. These results combined prove that the chemical and structural properties of the ink are a direct cause of its printability and reliability.

Part fabrication experiments also showed high dimensional fidelity, interlayer bonding and error-free geometry at the optimum conditions (390 mm/min, 60 ℃). This elaborate characterization confirms that the entire purpose of the research, formulation, rheological optimization, chemical compatibility, and structural uniformity, was indeed attained. Besides facilitating the process reproducibility and high printing resolution, the proposed LSR/TiO_2 composite ink allows expansion to stretchable and stitchable electronic parts, and biomedical elastomeric interfaces, where flexibility, dielectric; and mechanical stability is of primary importance. This study therefore lays a foundation towards scaled, multi-purpose DIW elastomeric systems that could be used in production of next generation flexible devices.

Funding

This research work did not receive any funding.

Data Availability Statement

Upon reasonable request, the corresponding author can provide the data used to justify the findings of this study.

Conflict of Interest

The authors confirmed that there is no conflict of interest in the publication of this research. Meanwhile, the financial or personal affiliations of the authors had no effect on the work reported in this paper.

REFERENCES

1. Foerster A, Annarasa V, Terry A, et al. UV-curable silicone materials with tuneable mechanical properties for 3D printing. Mater Des. 2021;205:109681.
2. Liu B, Ma B. 3D printing molding of UV-curing liquid silicone rubber by UV follow curing. J Appl Polym Sci. 2025;142:e56453.
3. Fay CD, Wu L. Cost-effective 3D printing of silicone structures using an advanced intra-layer curing approach. Technologies. 2023;11:179.
4. Young CA, O'Bannon M, Thomson SL. Three-Dimensional Printing of Ultrasoft Silicone with a Functional Stiffness Gradient. 3D Print Addit Manuf. 2024;11(2).
5. Senderoff DM. Biceps augmentation using solid silicone implants. Aesthet Surg J. 2018;38: 401–8.

6. McCoul D, Rosset S, Schlatter S, Shea H. Inkjet 3D printing of UV and thermal cure silicone elastomers for dielectric elastomer actuators. Smart Mater Struct. 2017;26:125022.
7. Davoodi E, Fayazfar H, Liravi F, et al. Drop-on-demand high-speed 3D printing of flexible milled carbon fiber/silicone composite sensors for wearable biomonitoring devices. Addit Manuf. 2020;32.
8. Luis E, Pan HM, Sing SL, et al. 3D Direct Printing of Silicone Meniscus Implant Using a Novel Heat-Cured Extrusion-Based Printer. Polymers (Basel). 2020;12:1031.
9. Liravi F, Toyserkani E. Additive manufacturing of silicone structures: A review and prospective. Addit Manuf. 2018;24:232–42.
10. Elizalde-Herrera FJ, Flores-Soto PA, Mora-Cortes LF, et al. Recent Development of Graphene-Based Composites for Electronics, Energy Storage, and Biomedical Applications: A Review. J Compos Sci. 2024;8:481.
11. Nieva-Esteve G, Agulló N, Grande-Molina M, et al. Developing tuneable viscoelastic silicone gel-based inks for precise 3D printing of clinical phantoms. Mater Adv. 2024;5:3706–20.
12. Yang G, Sun Y, Qin L, et al. Direct-ink-writing (DIW) 3D printing functional composite materials based on supra-molecular interaction. Compos Sci Technol. 2021;215:109013.
13. Qiao H, et al. Preparation and performance of Silica/epoxy group-functionalized biobased Elastomer nanocomposite. Ind Eng Chem Res. 2017;56:881–9.
14. Kim H, Kim J, Ryu K-H, et al. Embedded Direct Ink Writing 3D Printing of UV Curable Resin/Sepiolite Composites with Nano Orientation. ACS Omega. 2023;8:23554–65.
15. Ulfah IM, Raistuti Fidyaningsih, Sri Rahayu et al. Influence of carbon black and Silica Filler on the rheological and mechanical Properties of natural rubber compound. Procedia Chem. 2015;16:258–64.
16. Rius-Bartra JM, Ferrer-Serrano N, Agull N, et al. High-consistency silicone rubber with reduced Young's modulus. An industrial option to dielectric silicone rubber. J Appl Polym Sci. 2023;140:e54405.
17. Li J, Wu S, Zhang W, Ma K, Jin G. 3D printing of silicone elastomers for soft actuators. Actuators. 2022;11:200.
18. Neethirajan J, Parathodika AR, Hu G-H, et al. Functional rubber composites based on silica-silane reinforcement for green tire application: the state of the art. Funct Compos Mater. 2022;3:7.
19. Ortega JM, Golobic M, Sain JD, et al. Active Mixing of Disparate Inks for Multimaterial 3D Printing. Adv Mater Technol. 2019 Apr.
20. Duran MM, Moro G, Zhang Y, Islam A. 3D printing of silicone and polyurethane elastomers for medical device application: A review. Adv Ind Manuf Eng. 2023;7:100125.
21. Śliwiak M, Bui R, Brook MA, et al. 3D printing of highly reactive silicones using inkjet type droplet ejection and free space droplet merging and reaction. Addit Manuf. 2021;46:102099.
22. Bhattacharjee N, Urrios A, Kang S, et al. The upcoming 3D-printing revolution in microfluidics. Lab Chip. 2016;16:1720–42.
23. Koushki P, Kwok TH, Hof L, et al. Reinforcing silicone with hemp fiber for additive manufacturing. Compos Sci Technol. 2020;194:108139.
24. Amert RSA, Kellar JJ, Whites KW. Rheological Optimization and Stability Study of Silver Nano-Ink for InkJet Printing of Solar Electrodes Using Industrial Printhead. Cleantech. 2012.
25. Lee SJ, Yoon SJ, Jeon IY. Graphene/Polymer Nanocomposites: Preparation, Mechanical Properties, and Application. Polymers (Basel). 2022;14:4733.
26. Roh S, Parekh DP, Bharti B, et al. 3D Printing by Multiphase Silicone/Water Capillary Inks. Adv Mater. 2017;29(26):1701554.
27. Greenwood TE, Hatch SE, Colton MB, Thomson SL. 3D printing low-stiffness silicone within a curable support matrix. Addit Manuf. 2021;37:101681.
28. Miron VM, Lämmermann S, Çakmak U, et al. Material Characterization of 3D-printed Silicone Elastomers. Procedia Struct Integr. 2021;34:65–70.
29. Wang Y, Liu SY, Meng JS. Advanced materials for additive manufacturing. IOP Conf Ser Mater Sci Eng. 2019;479:012088.

30. Chen Y, Zhou L, Wei J, et al. Direct Ink Writing of Flexible Electronics on Paper Substrate with Graphene/Polypyrrole/Carbon Black Ink. J Electron Mater. 2019;48(9):5514–23.
31. Ahmed EM, Mostafa NY. Thermal stability, mechanical strength, and ionic conductivity of hematite nanoparticle/CS nanocomposites. Polym Polym Compos. 2025;33. doi:10.1177/09673911251327811.
32. Liu M, Zhao Y, Wang Y, et al. Design, simulations, and experiments of tube-making pultrusion process with glass fabric/PP composites. Polym Polym Compos. 2025;33. doi:10.1177/09673911251321020.
33. Aldakheel FM, Wickramasinghe R, Thamaraiselvan C, et al. Green silver nanoparticle-embedded chitosan-alginate hydrogel: A novel antibacterial approach for potential wound healing. Polym Polym Compos. 2025;33. doi:10.1177/09673911251320463.
34. Gahramanli L, Muradov M, Eyvazova G, et al. Comparison of the physical properties of CdxZn1-xS-based nanocomposite materials produced via sonochemical and SILAR approaches. Polym Polym Compos. 2025;33. doi:10.1177/09673911251318543.
35. Pandey R, Shrivastava AK, Mohan R, et al. A Review on Additive Manufacturing Processes. J Polym Compos. 2025;13(03):13–24.
36. Srividya DV, Vali SK, Hadya B, Sadaq SI. Failure Analysis of Hybrid Natural/Synthetic Fiber Composite Laminates in The Application of Hybrid Composite Pressure Vessel. J Polym Compos. 2025;13(03):85–98.
37. Venkatesh K, Rama Krishna LS, Kumar AS. Optimization of Process Parameters for FDM Printed Tensile Test Specimens to Reduce Energy Consumption and CO2 Emission for Sustainable Manufacturing. J Polym Compos. 2025;13(03):63–71.
38. Kumawat S, Yashpal, Jain NL. Fabrication of Belt for Backpack for Students to Reduce the Musculoskeletal Disorders using ABS material 3D Printing. J Polym Compos. 2024;13(01):1110–7.
39. Ananda MN, Reddy JS, Kumar SV, et al. Evaluation of Mechanical Properties of Carbon Reinforced Composite for Different Process Parameters Using FDM. J Polym Compos. 2024;11(13):218–28.
40. George M, George PP. Dielectric Properties of Reduced Graphene Oxide with Nickel Cobalt Ferrite and Nickel Zinc Ferrite Epoxy Nanocomposites. J Polym Compos. 2024;11(11):28–37.
41. Palanisamy S, Kalimuthu M, Palaniappan M, Alavudeen A, Rajini N, Santulli C, Al-Lohedan H. Characterization of Acacia caesia bark fibers (ACBFs). J Nat Fibers. 2021;19(15):10241–52. doi:10.1080/15440478.2021.1993493
42. Palanisamy S, Murugesan TM, Palaniappan M, Santulli C, Ayrilmis N. Use of hemp waste for the development of mycelium-grown matrix biocomposites: a concise bibliographic review. BioResources. 2023;18(4):8771–80. doi:10.15376/biores.18.4.Palanisamy
43. Padmanabhan RG, Rajesh S, Karthikeyan S, Palanisamy S, Ilyas RA, Ayrilmis N, Tag-eldin EM, Kchaou M. Evaluation of mechanical properties and Fick's diffusion behaviour of aluminum-DMEM reinforced with hemp/bamboo/basalt woven fiber metal laminates (WFML) under different stacking sequences. Ain Shams Eng J. 2024;15(7):102759. doi:10.1016/j.asej.2024.102759
44. Aruchamy K, Karuppusamy M, Krishnakumar S, Palanisamy S, Jayamani M, Sureshkumar K, Ali SK, Al-Farraj SA. Enhancement of mechanical properties of hybrid polymer composites using Palmyra palm and coconut sheath fibers: the role of tamarind shell powder. BioResources. 2025;20(1):698–724. doi:10.15376/biores.20.1.698-724
45. Ayrilmis N, Kanat G, Yildiz Avsar E, Palanisamy S, Ashori A. Utilizing waste manhole covers and fibreboard as reinforcing fillers for thermoplastic composites. J Reinf Plast Compos. 2024;44(17–18):1108–18. doi:10.1177/07316844241238507
46. Ramasubbu R, Kayambu A, Palanisamy S, Ayrilmis N. Mechanical properties of epoxy composites reinforced with Areca catechu fibers containing silicon carbide. BioResources. 2024;19(2):2353–70. doi:10.15376/biores.19.2.2353-2370

